African Journal of Biological Sciences

MAPPING OF HIGH LEVEL REMOTE SENSING IMAGE FEATURES WITH PIXEL DISTRIBUTION AND THRESHOLD COMPUTATION

R. Banupriya[1], N. M. Indumathi[2], A.Devendhiran , Navamani C[4]

[1]Department of Computer Science and Engineering, K.S.R College of Engineering, KSR Kalvi Nagar, Tiruchengode,Tamil Nadu - 637215,trbanupriya@gmail.com.

[2]Department of Computer Science and Engineering, Nandha College of Engineering(Autonomous) Erode, India.

[3]Department of Computer Science and Technology, Vivekanandha College of Engineering for Women (Autonomous), Tiruchengode.

[4]Department of Computer Science and Engineering, Nandha College of Engineering(Autonomous) Erode, India.

Abstract – In remote sensing images, extraction of high level features from flooded image captures the attention recent investigators. Moreover, higher level features attainment may lacks in high dimensionality and global representation. Here, thresholding and feature scaling are used for high level feature extraction. With a given input image dataset, image classification is performed with three diverse phases to extract features. As well, spatial index and scaling factors plays an essential role in this work. The results were validated using statistical measures like detection rate and false alarm rate on available datasets. Experiments on remote sensing image datasets demonstrate that the proposed mapping level shows higher progression towards classification performance. However, feature mapping outperforms the existing features extraction techniques from remote sensing images. Simulation is done with MATLAB environment and mapping of higher level features are extracted with level set analysis.

Index Terms- High level feature mapping, image classification, thresholding, remote sensing, factor scaling.

I. Introduction

Owing to various changes identified in land cover region and global changes, there is a clear rise in frequency and severity of flood over certain region [1]. Mapping of flooded region over a specific region is crucial for flood-based studies. Diverse multi-spectral remote sensing images are used for flood mapping phenomenon [2]. Moreover, certain spatial multi-spectral image resolution is harsh in high temporal resolution, However, numerous weather based flooding images may causes difficulties in gathering huge multi-spectral images this may

outcomes in coarse spatial resolution in multi-spectral images [3]. Generally, this crisis may results in mixed pixels. Mapping high resolution images are termed as sub-pixel mapping which is an effectual approach to resolve this crisis [4].

Mapping of spatial resolution method for unmixing spectral is based on spatial correlation theory. This may haul out sub-pixel distribution information inside combined by changing fractional images for mapping spatial resolution [5]. Various kinds of spatial attraction techniques have been used to specify spatial dependency to acquire mapping outcomes. Pixel swapping based methods has been anticipated to change sub-pixels classes which are essential in swapping mixed pixels [6]. Diverse techniques like hopefield neural network, indicator cokring, back propagation neural network and certain interpolation approaches which have been used for mapping spatial resolution [7]. To effectually perform spatial resolution based mapping using optimization procedures like particle swarm optimization, genetic algorithm and neural networks [8]. Moreover, spatial resolution techniques may generally used in spatial correlation to acquire flood mapping outcome and spectral information from multi-spectral remote sensing flood image bands are generally not used completely [9].

To overcome the problem specified above, this work considers mapping of high level features (MHLF) of spectral information is proposed. Differentiating normalized index with level set is quantified spectral indicator for characterizing the water bodies. MHLF has been extensively used in extracting water bodies through extraction of water information while reducing land information in those remote sensing images [10]. This investigation shows spectral information from various bands to compute MHLF. This spectral term is added to conventional mapping techniques. The experimental outcomes demonstrate that the proposed model shows better trade-off in contrast with other approaches for mapping more accurate results than other models. The remote sensing image view is shown in Fig 1. The significant contribution of the proposed model is given below:

1) To attain sub-pixel spatial flood distribution with various pixels for maximizing correlation between the pixels.
2) Acquire the class labels of pixels and scale factors are computed between sub-pixel and pixels.
3) Map the high level features using normalization factors.

The remainder of the work is organized as follows: Section II depicts background study and investigations related to mapping remote sensed images. Section III shows the proposed mapping strategy of high level features in detail, Section IV explains numerical outcomes attained for the computation of feature mapping. Finally, Section V gives the conclusion of the proposed mapping model with instructions for future research directions.
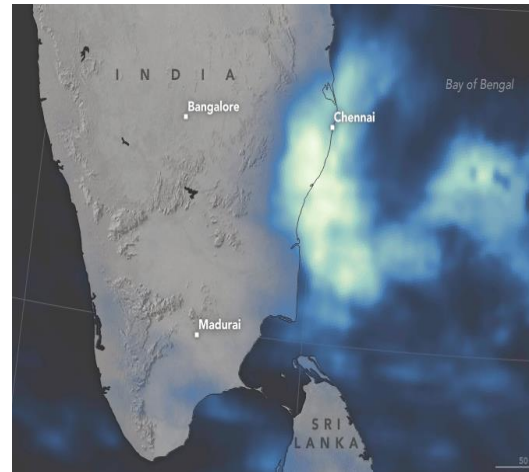

Fig 1: Satellite view of flooded region

II. Related works

The utilization of sensors for remote sensing images are considered as a crucial value added sources in flood mapping, owing to weather and image characteristics, fulfilling the acquisition availability of independent weather and illumination conditions [11]. Moreover, dealing with radar data for extracting information is considered typically with huge complexities by end-users this is often determined by more images attained from multi-spectral sensors [12]. This is because of both processing and interpretation issues; this principle is related to ability to work with radiometric factors that facilitates identification of numerous scene features via simple thresholding [13]. In surface water case, normalization differences with water index are stated by author in [14], which is a tool that has been extensively used in applications offered by comprehensible information during non-expert remote sensing based users.

Moreover, indeed of ease of use, multi-spectral data are generally not appropriate during emergency condition owing to illumination and weather sensitivity conditions [15]. Henceforth, scientific investigators are deeply analyzed by SAR data utilized. Thresholding-based technqiues have been anticipated, as an instance

provided in [16]. Author in [17], stated an integrated model for flood monitoring dependent on flood prediction and satellite acquisition exploitation. Author in [18], anticipated a flood prediction technqiue provided by satellite image acquisitions. Author in [19] explained bayesian network by merging ground information and other multi-temporal SAR data with geomorphic information. Usage of both unsupervised and supervised techniques and multi-modal data is analyzed in [20].

Author in [21], offered a fully automated functionalists for mapping flood by exploiting SAR-X data in pre-processing, initializing unsupervised model for classification and post-classification refinement for triggering satellite data delivery automatically. These techniques for flood depth estimation based on theoretical urban inversion scattering models were available in [21]. Author in [22] anticipated a model for exploiting SAR data in integration of Taguchi optimization and rule-based classification models. Variation identified in mapping flood in urban regions is considered by [23]. Author in [24], initiated by automatic split based thresholding procedure as effectual computation techniques offering appropriate outcomes in real time mapping. Author in [25], evaluated four operational SAR data for flood detection techniques. In global scale application, an automated water mapping procedure based long term training data set model to compute probability where pixel is merged by water provided in angle incidence and back scatter was given by [25].

Even though SAR images may follows more constant observation than that of optical imagery, water pixels classification may not be facilitated more straightly. Owing to specular reflectance properties of diverse water surfaces, these images may be seen as homogeneous and dark regions in SAR images. Moreover, wind may leads to roughness in water surface, therefore improving back-scatter responses with similar levels as neighbour-hood non-water pixel bodies. However, buildings and flooded vegetation may cause improved back-scattering levels owing to double bouncing factors and scattering volume within vegetation. These processes may be considered as complex technique for flood classification over cities and in densely vegetated regions. As well, protruding vegetation over flooded edge may leads to various crisis. In those regions, added complexities are encountered owing to layover effects that may hide flooded streets. Various other approaches may cause over-prediction. Owing to radar shadow effect that may reduce back-scatter signal from regions behind slopes or buildings that uses sensors, over-prediction may occur in cities or regions inside identical topography. Some parameters have to be considered during SAR-based development of flood mapping algorithm.

The volume and variety of literature are under investigation for addressing floods to testify surface water mapping from satellite images using spatial data is still an open crisis.

III. Proposed Methodology

This section considers three diverse phases: 1) pixel distribution of flooded images, 2) Threshold setting, 3) mapping high level features. The working function of the proposed model is given below in Fig 2.

a) Pixel distribution

For mapping, initially pixel distribution has to be considered in flooded regions within pixels. The spatial correlation between pixels has to be maintained with original flood properties within mixed pixels. Flood over remote sensing regions comprises of two classes known as flooded and non-flooded region. Fractional values specify flooded region proportion over the mixed pixels. It comprises of 3*3 mixed pixels and flooded region based proportional classes are specified in every mixed pixels. Scaling factor shows the scale ratio among sub-pixels and mixed pixels. When spatial unmixed results are upsampled with scale factor where s= 4, mixed pixel is partitioned into 4*4 sub-pixels. Here, 25% of these sub-pixels may come under flooded region in centre of mixed pixel. Consider spatial correlation principle where the most likely outcomes are attained from highest spatial correlation. Henceforth, close optimality of proposed model is discusses below:

The mapping of high resolution pixels are formulated based on spatial correlation principle. The spatial index of flooded region is considered to compute spatial correlation between centre region of sub-pixels p_i $(i = 1,2 \dots, MS^2)$ and neighbourhood of mixed pixels. This is mathematically provided below in Eq. (1):

$Spatial\ Indexing$

$$= o_i . \sum_{C=1}^{M_n} w_i C . L(P_C) + (1 - o_i) . \left[\sum_{C=1}^{M_n} w_i C . \left(1 - L(P_C) \right) \right]$$

Where o_i is labels of sub-pixels (1 for flooded and 0 for non-flooded region based labels). $L(P_c)$ is flooded class label proportion for neighbourhood mixed pixels. P_C and M_n is mixed number of neighbourhood pixels. Maximal of eight neighbourhood pixels are considered in this work.

w_{iC} is weighted dependency among neighbourhood pixels and central sub-pixels. It is expressed as in Eq. (2):

$$w_{ic} = \exp(-\frac{d(p_i, P_C)^2}{r})$$

Where $d(p_i, P_C)$ Euclidean distance from central sub-pixel is position p_i to neighbourhood pixel and $'r'$ is non-linear exponential model based parameter. Index of all sub-pixels are provided as spatial measures and computed as below in Eq. (3):

$$E(i) = Max \sum_{i=1}^{MS^2} spatial\ index$$

Spatial resolution of evaluation criteria are measured as higher (), superior probability of sub-pixel distribution, Henceforth, this may be assigned as flooded region label to sub-pixels while maximizing the values.

b. Thresholding remote sensing region

Based on existing approach, global thresholding is known for its fast and simple computation. However, it suffers from certain drawbacks. This is due to the negligence of spatial content of image pixels. Therefore, it needs some further processing. However, threshold-based performance may highly influenced by the contrast and size of full sized image between non-flooded and flooded pixels. Specifically, if flooded region pixel proportion is smaller, due to water roughening thresholding may be introduced with some errors. To address this issue, various investigators concentrated on determining selective region for threshold selection. The tiles of remote sensing image has been sub-divided into tiles and corresponding tiles are specifies with bimodal histogram for threshold selection. With split based model, image is partitioned into non-overlapping pixels are partitioned into sub-pixels. For every pixel, mean and standard deviation of sub-pixels are computed first. Pixel selection may have standard deviation of sub-pixels with 95% higher percentage and lower mean of all pixels. If pixel selection is empty, pixel dimensions are

halved and this process will be repeated. Based on this selection, 'N' pixels may have highest SD of pixel means to be withheld. At last, thresholding is provided as a mean of threshold from chosen pixels. SD of selected pixels is used as a quality indicator. If value is higher than 5.0-6.0 dB, sub-pixels of chosen pixels are merged into histogram and it is provided based on this histogram. The significant use of quality indicator or indices is to eliminate the false selection of bi-model pixels, i.e. bi-modality occurs due to bounce outliers.
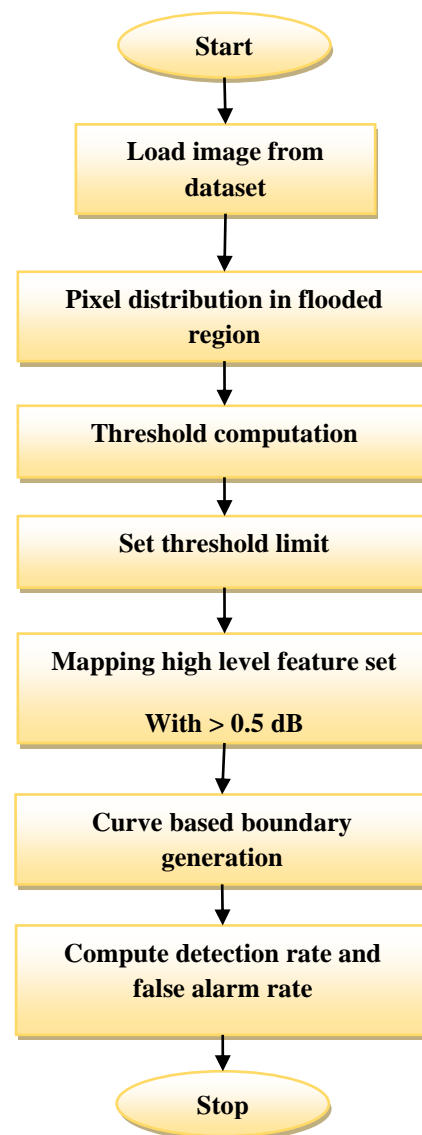
```
        ┌─────────────┐
        │    Start     │
        └──────┬──────┘
               ▼
      ┌──────────────────┐
      │ Load image from   │
      │ dataset           │
      └────────┬─────────┘
               ▼
    ┌──────────────────────┐
    │ Pixel distribution in │
    │ flooded region         │
    └──────────┬───────────┘
               ▼
    ┌──────────────────────┐
    │ Threshold computation │
    └──────────┬───────────┘
               ▼
    ┌──────────────────────┐
    │ Set threshold limit   │
    └──────────┬───────────┘
               ▼
    ┌──────────────────────┐
    │ Mapping high level    │
    │ feature set            │
    │ With > 0.5 dB          │
    └──────────┬───────────┘
               ▼
    ┌──────────────────────┐
    │ Curve based boundary  │
    │ generation             │
    └──────────┬───────────┘
               ▼
    ┌──────────────────────┐
    │ Compute detection     │
    │ rate and false alarm   │
    │ rate                   │
    └──────────┬───────────┘
               ▼
        ┌─────────────┐
        │    Stop      │
        └─────────────┘
```

Fig 2: Flow diagram of proposed model

To demonstrate modality regions within certain region, varying pixel size and Ashman coefficient for pixel selection is provided here. The mathematical computation of this ashman coefficient is given in Eq.(4):

$$A(h) = \sqrt{2}\frac{|\mu_1 - \mu_2|}{\sqrt{\sigma_1^2 + \sigma_2^2}}$$

Where μ_1 are means and σ_1 and σ_2 standard deviation, $'h'$ is histogram respectively. If coefficients are higher, then separability of two distributions is more significant. The coefficient value should be higher than 2, so as to ensure separability. This co-efficiency is measured with two classes as determined by pixel threshold. Image size of 200*200 is considered based on experimental outcomes indeed of pixel size between 150*150 and 400*400. To enhance the contrast among flooded and non-flooded regions, index has to be computed with higher differences among the flooded region and drained region outlets over sensing region. The threshold is set for masking but not prone to flooding over certain region. Therefore, the threshold region is set for 15m. Most of the existing thresholding approaches are merged with pre-processing techniques to eliminate unknown water like surface. This is performed with data like land cover information, topography and mask. Some methods may consist of removal of small objects. This work directly concentrates on extracting higher level features from flooded region for mapping purpose. Therefore, classifiers may work effectually with these outcomes.

c. High level feature mapping

Consider Ω is domain of flooded image partitioning into sub-domains with curve. Assume probability density function of image domain with 3*3 complex random covariance matrix which is included in every image pixel X. To have topological analysis, two factors have to be considered slope and energy function. Energy function is provided as below in Eq. (5):

$$E\big(\Omega_1, \Omega_2 D(X), S(X)\big)$$
$$= -\ln\left\{\sum_{i=1}^{2} \lambda_i \int_{\Omega_i} P(D(X)|\Omega_i)d\Omega\right.$$
$$\left. + \omega_i \int_{\Omega_i} S(X|\Omega_i)d\Omega + \mu \int g(X)ds\right\}$$

Where $S(X|\Omega_i)$ is mean image slope, Ω_i and w_i is constant number. This slope item may have topological sensitivity and eliminate non-flooded region in slope which is generally higher than water. The flooded curves are provided as a level set function. Curve 'C' is determined as edge of image as Ω is zero level set function at $t(t = 0)$ moment. Level set based evolution scheme is resolved to reducing energy function. Zero initial curves level set evolution more effectually and

precisely. Variation is modelled by curve generation to specify initial curve, this focuses on spatial relationship between permanent waters when initializing zero level curve set. This plays a role in zero initial level curve set. The flooded scenario is explained in Eq. (6):

$$\emptyset_o\big(\mu(x,y)\big)$$
$$= pow\big(\mu(x,y)\big)$$
$$- \delta\big(dist_B\big(\mu(x,y), \mu_0(x_0, y_0)\big)\big)$$

Where pow is flooded image power and $Dist_B(\mu(x,y), \mu(x_0, y_0))$ is mean function. $\mu(x,y)$ is distance between pixel segmented and corresponding pixel $\mu_0(x_0, y_0)$ of flooded image.

IV. Numerical results and discussions

The performance evaluation is done with MATLAB simulation environment. With huge amount of existing flood mapping approaches, this work attempts to profoundly increase flood mapping with improved robustness and accuracy. The input images are processed based on the procedures given above. The robustness of proposed model is evaluated with sub-set pixel values. To improve classification accuracy, various performance metrics are available. These are computed based on confusion matrix. This matrix format shows how many pixels are under-estimated, over-estimated, correctly classified. These metrics are used to evaluate the multiple class classification, i.e. mapping of flooded region. With two class classification problem with flood mapping, accuracy of flooded and non-flooded class.
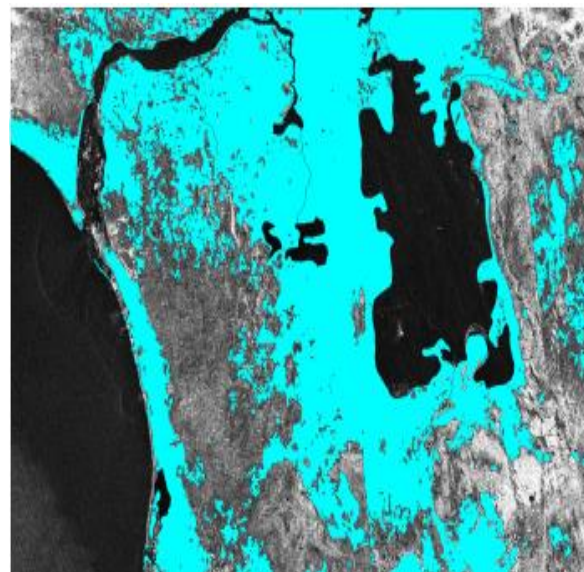

Fig 3: Input sample 1

In flood classification, non-flooded class are generally background class and much higher than flooded class. When using the global threshold concept, it is termed as proportion correction; the performance is measured to be highly sensitive when considering the non-flooded region and directly due to subset pixels. If the non-flooded area is higher, then it is known as over estimated region. As an outcome, the indices do not measure appropriately classified non-flooded pixels. The index value provides superior indication regarding the global accuracy of flood classification; however it may not provide any data related to over-prediction and under-prediction with spatial distribution errors. Therefore, the accuracy of the proposed model is based on index. The threshold and area specification are based on dataset validation. This is used to compute changes encountered in detection process.
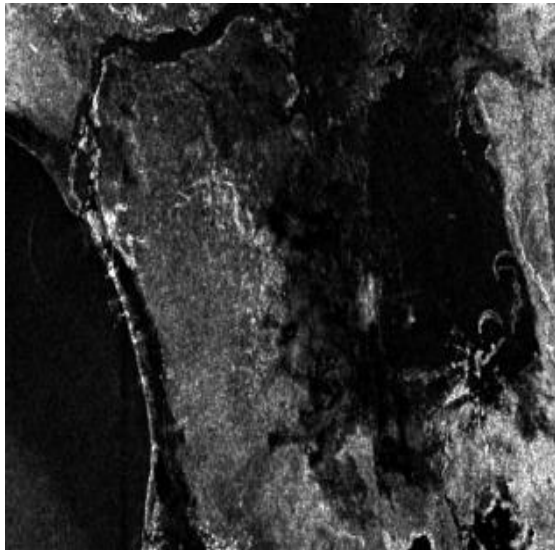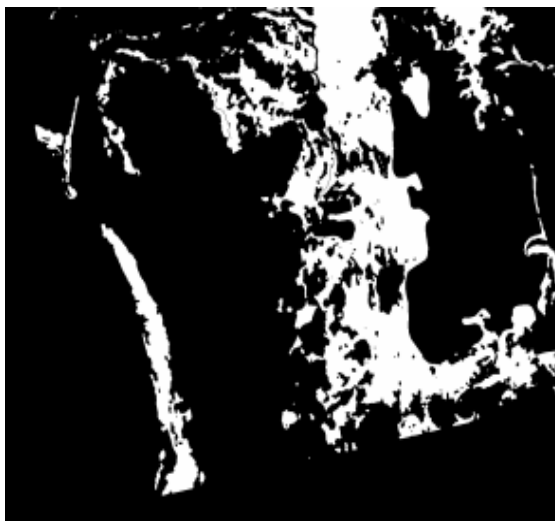

Fig 4: Image scaling factor 1

Fig 5: High level feature mapping 1

The classification outcomes are measured with various thresholding approaches. It is completely dependent on two classes and related histogram bimodalities. Generally, the performance reduces with rise in subset size of threshold algorithms. Global thresholds are more accurate for subset pixels and reduce the performance when bimodality disappears. The contrast between non-flooded and flooded pixels in images is extremely lower, which leads to impossibly to separate two classes by simple threshold. However, some algorithm may provide acceptable performance when given to LandSat images. Owing to unequal size of classes, larger class of non-flooded pixel is partitioned and non-flooded class is classified as flood region. Flooded region of higher size may leads to higher performance. When using this threshold for image analysis, it is essential to eliminate border with darker pixels which causes stronger threshold predictions and flooded region. Images may show unrealistic thresholds (>0 dB) and strong bias that results in global thresholding. For instance, it is essential for selecting both procedures. The sample image analysis and processing is done in Fig 3- Fig 8.
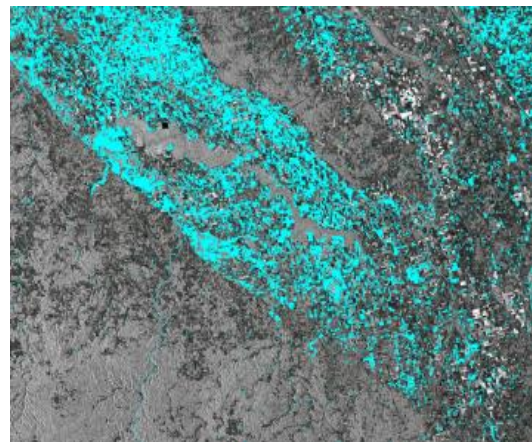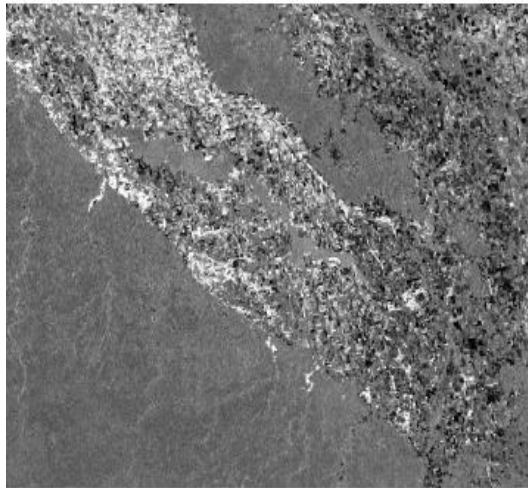

Fig 6: Input sample 2

Fig 7: Image scaling factor 2

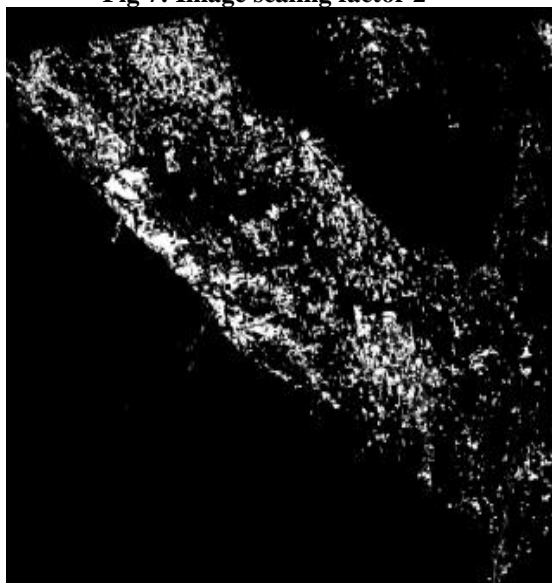**Detection rate**

Fig 9: Detection rate

Fig 8: High level feature mapping 2

Detection of flooded and non-flooded region may rely over variation in prediction process. The added information regarding non-flooded image may limits water surface over-prediction and facilitates flooded surface detection with permanent water bodies in final classification. The minimal flooded objects are set as 0 pixels. The algorithm works well for all image pairs over every subsets and may not reduces the functionality even in case of applying it to entire image processing.
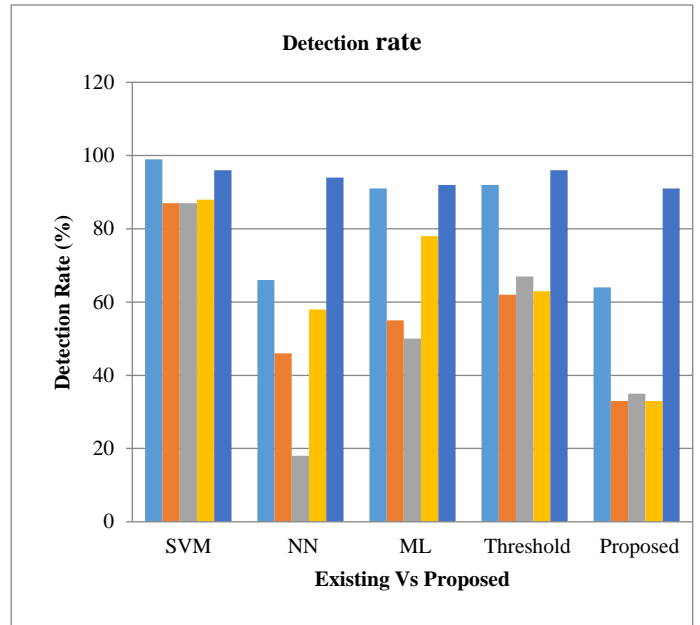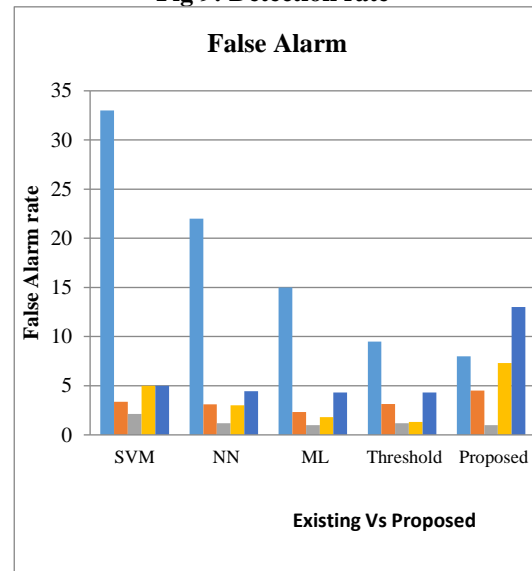
Fig 10: False alarm rate

Table I: Detection rate and False alarm computation

SVM		NN		ML		Thresh old		Propos ed	
D R	FA	D R	FA	D R	FA	D R	FA	D R	FA
9 9	33	8 7	22	8 7	15	8 8	9.5 0	9 6	8
6 6	3. 36	4 6	3. 10	1 8	2. 31	5 8	3.1 3	9 4	4. 50
9 1	2. 13	5 5	1. 17	5 0	1	7 8	1.2 0	9 2	1
9 2	5	6 2	3. 01	6 7	1. 80	6 3	1.3 0	9 6	7. 30
6	5	3	4.	3	4.	3	4.3	9	13

4		3	45	5	30	3	1	1	.0
8	9.	5	6.	5	4.	6	3.9	9	6.
2	80	7	90	1	90	6	0	5	85

Fig 9 and Fig 10 shows the graphical representation of detection rate and false alarm rate as performance metrics. Table I shows the numerical values of the proposed model. This work shows the mapping of features more appropriately when compared to existing approaches like SVM, NN, ML, Thresholding techniques.

V. Conclusion

This section discusses in detail about the flood detection model from LandSat/remote sensing images with high resolution images for mapping higher level features for detecting the boundaries more appropriately. This mapping helps in determining higher level features that shows superior flood based boundary maintenance. This work projects the in-depth evaluation and assessment for establishing flood boundaries with higher level feature mapping. This is further divided into three categories: pixel distribution, thresholding and higher level feature mapping. Effectual mapping of flooded region is considered as a crucial approach for effectual response implementation. The scaling factors, euclidean distance are some measures that are considered for computation. The output mapping shows higher resolution on image pixel estimation. The performance of the proposed model is compared with existing approaches and shows better outcomes for rapid mapping of flood to assist the response of proposed model.

In future, segmentation and mapping of high level features to enhance the classification outcomes.

REFERENCES

[1] P. Dimitriadis *et al.*, "Comparative evaluation of 1D and quasi-2D hydraulic models based on benchmark and real-world applications for uncertainty assessment in flflood mapping," *J. Hydrol.*, vol. 534, pp. 478–492, Mar. 2016.

[2] F. Ling, Y. Du, Y. Zhang, X. Li, and F. Xiao, "Burned-area mapping at the subpixel scale with MODIS images," *IEEE Geosci. Remote Sens. Lett.*, vol. 12, no. 9, pp. 1963–1967, Sep. 2015.

[3] P. Wang, L. Wang, Y. Wu, and H. Leung, "Utilizing pansharpening technique to produce sub-pixel resolution thematic map from coarse remote sensing image," *Remote Sens.*, vol. 10, no. 6, p. 884, Jun. 2018.

[4] X. Li, Y. Du, F. Ling, Q. Feng, and B. Fu, "Superresolution mapping of remotely sensed image based on Hopfifield neural network with anisotropic spatial dependence model," *IEEE Geosci. Remote Sens. Lett.*, vol. 11, no. 7, pp. 1265–1269, Jul. 2014.

[5] P. Wang, G. Zhang, and H. Leung, "Utilizing parallel networks to produce sub-pixel shifted images with multiscale spatio-spectral information for soft-then-hard sub-pixel mapping," *IEEE Access*, vol. 6, no. 1, pp. 57485–57496, Oct. 2018.

[6] L. Li, Y. Chen, X. Yu, R. Liu, and C. Huang, "Sub-pixel flflood inundation mapping from multispectral remotely sensed images based on discrete particle swarm optimization," *ISPRS J. Photogramm. Rem. Sens.*, vol. 101, pp. 10–21, Mar. 2015.

[7] H. Xie, X. Luo, X. Xu, H. Pan, and X. Tong, "Automated subpixel surface water mapping from heterogeneous urban environments using Landsat 8 OLI imagery," *Remote Sens.*, vol. 8, no. 7, p. 584, Jul. 2016.

[8] D. Amitrano *et al.*, "Urban areas enhancement in multitemporal SAR RGB images using adaptive coherence window and texture information," *IEEE J. Sel. Topics Appl. Earth Observ. Remote Sens.*, vol. 9, no. 8, pp. 3740–3752, Aug. 2016

[9] D'Addabbo, A. Refifice, G. Pasquariello, F. P. Lovergine, D. Capolongo, and S. Manfreda, "A Bayesian network for flood detection combining SAR imagery and ancillary data," *IEEE Trans. Geosci. Remote Sens.*, vol. 54, no. 6, pp. 3612–3625, Jun. 2016.

[10] Donchyts, J. Schellekens, H. Winsemius, E. Eisemann, and N. van de Giesen, "A 30 m resolution surface water mask including estimation of positional and thematic differences using Landsat 8, SRTM and OpenStreetMap: A case study in the Murray-Darling basin, Australia," *Remote Sens.*, vol. 8, no. 5, p. 386, 2016

[11] Amitrano, G. D. Martino, A. Iodice, D. Riccio, and G. Ruello, "Small reservoirs extraction in semiarid regions using multitemporal synthetic aperture radar images," *IEEE J. Sel. Topics Appl. Earth Observ. Remote Sens.*, vol. 10, no. 8, pp. 3482–3492, Aug. 2017.

[12] Giustarini, R. Hostache, P. Matgen, G. J.-P. Schumann, P. D. Bates, and D. C. Mason, "A change

detection approach to flflood mapping in urban areas using TerraSAR-X," *IEEE Trans. Geosci. Remote Sens.*, vol. 51, no. 4, pp. 2417–2430, Apr. 2013

[13] Long, T. E. Fatoyinbo, and F. Policelli, "Flood extent mapping for Namibia using change detection and thresholding with SAR," *Environ. Res. Lett.*, vol. 9, no. 3, pp. 35002–35009, 2014.

[14] Grimaldi, Y. Li, V. R. N. Pauwels, and J. P. Walker, "Remote sensingderived water extent and level to constrain hydraulic flflood forecasting models: Opportunities and challenges," *Surv. Geophys.*, vol. 37, no. 5, pp. 977–1034, 2016.

[15] Chow, A. Twele, and S. Martinis, "An assessment of the Height Above Nearest Drainage terrain descriptor for the thematic enhancement of automatic SAR-based flflood monitoring services," *Proc. SPIE*, vol. 9998, p. 999808, Oct. 2016.

[16] Bioresita, A. Puissant, A. Stumpf, and J.-P. Malet, "A method for automatic and rapid mapping of water surfaces from sentinel-1 imagery," *Remote Sens.*, vol. 10, no. 2, p. 217, 2018

[17] Stephens, G. J.-P. Schumann, and P. D. Bates, "Problems with binary pattern measures for flflood model evaluation," *Hydrol. Process.*, vol. 28, no. 18, pp. 4928–4937, 2014.

[18] Gobeyn *et al.*, "Impact of the timing of a SAR image acquisition on the calibration of a flflood inundation model," *Adv. Water Resour.*, vol. 100, pp. 126–138, Feb. 2017

[19] Matgen, R. Hostache, G. J.-P. Schumann, L. Pfifister, L. Hoffmann, and H. H. G. Savenije, "Towards an automated SAR-based flood monitoring system: Lessons learned from two case studies," *Phys.*

Chem. Earth A/B/C, vol. 36, nos. 7–8, pp. 241–252, 2011.

[20] Giustarini, R. Hostache, P. Matgen, G. J.-P. Schumann, P. D. Bates, and D. C. Mason, "A change detection approach to flflood mapping in urban areas using TerraSAR-X," *IEEE Trans. Geosci. Remote Sens.*, vol. 51, no. 4, pp. 2417–2430, Apr. 2013.

[21] Lu, J. Li, G. Chen, L. Zhao, B. Xiong, and G. Kuang, "Improving pixel-based change detection accuracy using an object-based approach in multitemporal SAR flflood images," *IEEE Trans. Geosci. Remote Sens.*, vol. 8, no. 7, pp. 3486–3496, Jul. 2015.

[22] Sui, C. Xu, J. Liu, K. Sun, and C. Wen, "A novel multi-scale level set method for SAR image segmentation based on a statistical model," *Int. J. Remote Sens.*, vol. 33, no. 17, pp. 5600–5614, 2012.

[23] Sui, C. Xu, J. Liu, K. Sun, and C. Wen, "A novel multi-scale level set method for SAR image segmentation based on a statistical model," *Int. J. Remote Sens.*, vol. 33, no. 17, pp. 5600–5614, 2012.

[24] Shi, P. Li, J. Yang, and L. Zhao, "Refifined land-cover classifification algorithm in airborne POLSAR system," *J. Remote Sens.*, vol. 16, no. 6, pp. 1130–1144, 2012

[25] Jin, G. Mountrakis, and P. Li, "A super-resolution mapping method using local indicator variograms," *Int. J. Remote Sens.*, vol. 33, no. 24, pp. 7747–7773, Jul. 2012.